UDC 532.517:537.584

A DYNAMO MODEL IN A SPHERICAL SHELL

M. Reshetnyak[1] and B. Steffen[2]

For the convection-driven dynamo in the Boussinesq approximation in a rotating spherical shell, we study various regimes of thermal convection which may occur in the planetary cores. Our dynamo model is based on the control volume method, which is well suited for parallel computers using message passing. We consider different boundary conditions at the surface of the shell and mimic a regime with stratification, which is typical for compositional convection. The influence of the inner solid conductive core on reversals is considered. Applications of our modeling to the two different planetary geometries — the Earth and Giant planets — are discussed.

1. Introduction. It is believed that the magnetic field in various astrophysical objects is maintained by the motions of either an ionized plasma, as it is the case in the galaxies or in the stars (see, e.g., [1]), or of a conductive fluid, as in the cores of the planets [2]. The description of this magnetohydrodynamic problem is the subject of the dynamo theory. In contrast to the solar or galaxy dynamo, where the magnetic field may be rather weak and has little effect on the flow, the dynamo in the planets and its satellites is strong enough to make the process nonlinear. In these objects, the Lorentz force is comparable with the other forces. Therefore, planetary dynamos are highly complicated and the usual method of investigation is numerical simulations. Since the magnetic field generation is a three-dimensional process, reasonable results were obtained only after appearing the modern supercomputers [3, 4].

If ten years ago, the main aim of geodynamo simulations was to obtain any self-consistent dynamo solution, now we have a variety of such solutions; therefore, a thorough analysis of the bulk of 3D-simulated data as well as the parameters in use is needed. This necessity is also reinforced by the uncertainty of details of the inner Earth and by the much larger uncertainty of physical models for the interior of other planets.

Here we propose a new multiprocessor version of the control volume geodynamo code (see for details of the algorithms in [5, 6]). We consider the parameters corresponding to different regimes of thermal convection in spherical shells of various thickness. For this reason, we study a set of thermal boundary conditions and a regime with stratification. We show that the change of the relative strength of the Coriolis force leads to the magnetic field morphologies typical for the geodynamo or the Giant planet dynamos.

The other aim of this modeling is to consider the magnetic field distribution during the reversals of the magnetic field and to estimate the correlation of the magnetic field behavior at the surface of a planet and in its inner conductive solid core. Some years ago, the stabilizing role of the inner core on the reversals raised no doubts [7], but now its influence is believed to be just some change of the convection and the damping of the fast reversals with a typical time of less than 10^3 years [8].

2. Basic equations.

2.1. The mathematical problem. The dynamo process driven by the flows of an incompressible fluid ($\nabla \cdot \mathbf{V} = 0$) in the Boussinesq approximation during the spherical ($r_{\mathrm{ICB}} \leqslant r \leqslant r_{\mathrm{CMB}}$) rotation[3] with an angular velocity Ω is described (see, e.g., [3]) by the induction equation

$$\frac{\partial \mathbf{B}}{\partial t} = \nabla \times \big(\mathbf{V} \times \mathbf{B}\big) + \mathrm{q}^{-1} \nabla^2 \mathbf{B}, \tag{1}$$

by the Navier–Stokes equation

$$\mathrm{Pr}^{-1}\,\mathrm{E}\left(\frac{\partial \mathbf{V}}{\partial t} + \big(\mathbf{V} \cdot \nabla\big)\mathbf{V}\right) = -\nabla P + \mathbf{F} + \mathrm{E}\,\nabla^2 \mathbf{V}, \tag{2}$$

[1] Institute of the Physics of the Earth, Russian Acad. Sci., 123995 Moscow, Russian Federation; e-mail: maxim@uipe-ras.scgis.ru; Research Computing Center of Moscow State University, 119992, Moscow, Russian Federation; e-mail: rm@uipe.srcc.msu.su

[2] Central Institute for Applied Mathematics (ZAM) of Forshungszentrum Jülich, D-52425, Jülich, Germany; e-mail: b.steffen@fz-juelich.de

[3] In what follows, by r_{ICB} and r_{CMB} we denote the inner core boundary (ICB) and the core-mantle boundary (CMB), respectively, as is customary in geodynamo.

and by the heat-flux equation with the heat sources $G(r)$:

$$\frac{\partial T}{\partial t} + (\mathbf{V} \cdot \nabla)T = \nabla^2 T + G. \tag{3}$$

These equations are scaled with the shell's outer radius L, which makes the dimensionless radius $r_{\mathrm{CMB}} = 1$; the inner core radius r_{ICB} is equal to 0.35 (like the radius of the Earth). The velocity $\mathbf{V}$, the magnetic field $\mathbf{B}$, the pressure P, and the typical diffusion time t are measured in units of $\frac{\kappa}{L}$, $\sqrt{2\Omega\kappa\mu\rho}$, $\frac{\rho\kappa^2}{L^2}$, and $\frac{L^2}{\kappa}$, respectively, where κ is the thermal diffusivity, ρ is the density, μ is the permeability, $\mathrm{Pr} = \frac{\kappa}{\nu}$ is the Prandtl number, $\mathrm{E} = \frac{\nu}{2\Omega L^2}$ is the Ekman number, ν is the kinematic viscosity, η is the magnetic diffusivity, and $\mathrm{q} = \frac{\kappa}{\eta}$ is the Roberts number.

The force $\mathbf{F}$ includes the Coriolis, Archimedean and Lorentz effects:

$$\mathbf{F} = -\mathbf{1}_z \times \mathbf{V} + \mathrm{Ra}\ Tr\, \mathbf{1}_r + (\nabla \times \mathbf{B}) \times \mathbf{B}, \tag{4}$$

where (r, θ, φ) is the spherical coordinate system, $\mathbf{1_z}$ is the unit vector along the axis of rotation, $\mathrm{Ra} = \frac{\alpha g_o \delta T L}{2\Omega\kappa}$ is the modified Rayleigh number, α is the coefficient of volume expansion, δT is the unit of temperature (see for more details [3]), and g_o is the gravitational acceleration at $r = r_{\mathrm{CMB}}$.

The inner core ($r \leqslant r_{\mathrm{ICB}}$) with the surface S_{ICB} can rotate about the z-axis due to the viscous and magnetic torques τ. The momentum equation for the angular velocity ω of the inner core is of the form

$$\mathrm{E}\ I\, \frac{\partial \omega}{\partial t} = \mathrm{Pr}\ r_{\mathrm{ICB}} \oint\limits_{S_{\mathrm{ICB}}} \tau_{r\varphi} \sin\theta \, \mathrm{d}S, \tag{5}$$

where I is the moment of inertia of the inner core; the stress-tensor components are defined as

$$\tau_{r\,\varphi} = \mathrm{E}\left(\frac{\partial V_\varphi}{\partial r} + \frac{1}{r\sin\theta}\,\frac{\partial V_r}{\partial \varphi} - \frac{V_\varphi}{r}\right) + B_r B_\varphi \sin\theta.$$

The conductivity of the inner core is assumed to be the same as of the liquid part.

2.2. A numerical model. Eqs (1) – (5) were successfully solved using, mostly, the poloidal and toroidal decompositions and the spectral numerical methods [9]. The origin of such a decomposition technique goes back to the mean-field dynamo theory [10], where many analytical results were obtained by means of these decompositions. There is no doubt that, for laminar flow and regular boundaries, the spectral methods give superior resolution and accuracy. For the regimes of fully-developed turbulence with space-dependent coefficients in the partial differential equations (as well as for the solutions with discontinuities or boundary layers), however, the application of grid methods and primitive physical variables may be preferable. The other advantage of the numerical methods that deal with variables in the physical space is their easy implementation on parallel computers. The numerical methods used in hydrodynamics for the variables in the physical space can be roughly divided into the three groups: the finite difference, finite volume, and finite element methods. The first group is the simplest in discretization and programming, but for the spherical system of coordinates, it meets serious stability troubles when the minimal distance between the points is $\sim \delta r\, \delta\theta\, \delta\varphi$ as $r \to 0$ and $\theta \to 0,\ \pi$ in the case of a regular grid with mesh steps $(\delta r,\ \delta\theta,\ \delta\varphi)$. Thus, even the application of methods fully implicit in time shows poor convergence.

The finite element methods are useful if the convective volume has an irregular boundary and the adaption of the system of coordinates is not feasible. In this case, the geometric flexibility of finite elements compensates any overhead involved. For spherical symmetrical problems, like the planetary dynamo, the extra complications involved give no benefit and such methods are rarely used.

In this paper we use the finite volume (or control volume) method developed by Patankar [11]. This method used usually for the thermal convection problems in the Cartesian geometry was recently applied with success to the geodynamo problem in a rotating sphere [5, 6]. The main advantage of this method over the finite difference method is that the dynamo problem is formulated in terms of fluxes. If the fluxes at the zero surfaces of control volumes in the center or at the axis are zero (which is, of course, equivalent to the natural assumption that all velocities are finite), no additional boundary conditions are needed (see [5] for details).

2.3. Parallelization. For the implementation of the model (2) – (5) on a grid of size M^3 (say, $M \sim 10^2$) on a supercomputer, the single-processor MHD code [5, 6] was improved to a multiprocessor version.

For this purpose, we applied the MPI library tools for communication, which makes the code independent of the computer architecture. In order to parallelize the program, the volume of the whole sphere was divided into $(\mathrm{N}_\theta \times \mathrm{N}_\varphi)$ $(\mathrm{N} = \mathrm{N}_\theta = \mathrm{N}_\varphi = 3 \div 5)$ slices in the two angular directions (θ and φ), so that eqs (1) – (5) were solved on each processor simultaneously. Two additional processors were reserved for synchronization of the processes and for input-output operations. The exchange operations between the different processors require passing of two-dimensional surface arrays to the neighbor subvolumes.

The code was tested on computer systems of different architectures, such as PC clusters as well as a multiprocessor IBM supercomputer with the shared memory for 32 processors each. For the tested values of M and $N = 5$, the communication required about 15% of the total time, revealing acceptable efficiency of parallelization.

3. Results of simulations. To model different thermal regimes of convection, we rewrite the convective term of the heat-flux equation in "homogeneous" form. For this purpose, we divide the temperature into two parts: $T = T_0 + T'$, so that $\nabla^2 T_0 = -G(r)$. Then, instead of Eq. (3) we obtain the following equation for the perturbation T':

$$\frac{\partial T'}{\partial t} + (\mathbf{V} \cdot \nabla)\,(T_0 + T') = \nabla^2 T'. \tag{6}$$

Eq. (6) has the homogeneous boundary conditions of the same kind as the original equation (3). This approach is very convenient from the numerical point of view [12] and does not influence the solution of the system (1), (2), (4), (5), what was checked in our tests. Below we consider various spherically symmetric thermal boundary conditions (see for details of regimes with inhomogeneous boundary conditions in [13]).

3.1. Fixed temperature at ICB & CMB. Regime I. Traditionally, the simplest thermal regime considered in the dynamo models has two prescribed boundary temperatures (heating below, $T_{\mathrm{ICB}} > T_{\mathrm{CMB}}$) and $G = 0$. Let $T_{\mathrm{ICB}} = -1$ and $T_{\mathrm{CMB}} = 0$. Then (see Figure 1) $T_0 = -\dfrac{1 - r/r_{\mathrm{ICB}}}{1 - r_{\mathrm{ICB}}}$ and $T'_{\mathrm{ICB}} = T'_{\mathrm{CMB}} = 0$.

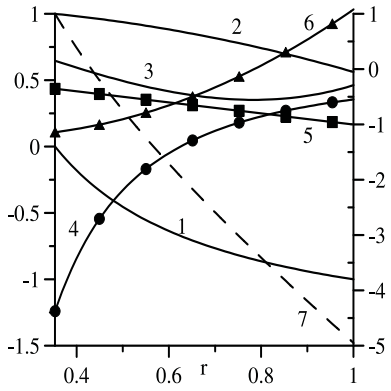

Fig. 1. Temperature profiles T_0 (left axis) — 1, 2, 3 and its gradient, ∇T_0 (right axis, lines with labels) — 4, 5, 6 for Regimes I, II, III, respectively. The dotted line (left axis) is the normalized density of the heat sources $G(r)/5.37$ in Regime III

In contrast to the other thermal regimes (see below), this regime provides the maximal gradient of the temperature field near ICB[4]. In its turn, vigorous convection in this region generates a strong dipole magnetic field, which is characteristic for the geodynamo. Therefore, these conditions are often applied in simulations. For this regime, the evolution of some selected integral quantities is presented in Figure 2 for $\mathrm{E} = 3 \cdot 10^{-3}$, $\mathrm{Pr} = 1$, $\mathrm{Ra} = 10^3$, and $\mathrm{q} = 2$ on the grid $(35 \times 35 \times 40)$ with $3 \times 3 + 2$ processors.

The mean level of the kinetic energy E_k for this regime is similar to that of the magnetic energy E_m (the equipartition state). This is a typical situation for regimes with moderate rotation. To reach a superbalance regime, where the magnetic energy (as it is believed to be in the Earth' core) is orders of magnitude larger than the kinetic energy, one needs a smaller E, which in its turn requires the application of superdiffusion [14] or a much finer grid. However, the existence of superbalance is a very tricky point, whereas a role of the Lorentz force in the dynamo process is not clear. It follows from [3] that the magnetic field does not change the form of the convective structures too much (the magnetic field appears to be force-free) and its influence is reduced to appearing of additional quasiperiodic oscillations. At the same time, reversals of magnetic field can be described in terms of the pure kinematic problem [15] with the same parameters as in the full problem and with the same initial conditions for at least some diffusion times. It is worth noting that for the first 14 harmonics at least the

[4]Note that an increase of the Prandtl number gives the same effects.

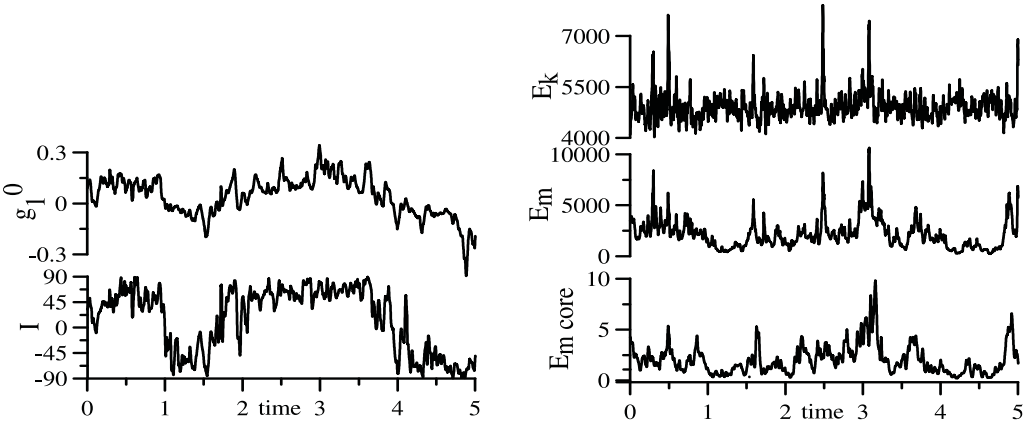

Fig. 2. Regime I, $\mathrm{E} = 3 \cdot 10^{-3}$, $\mathrm{Pr} = 1$, $\mathrm{Ra} = 10^3$, $\mathrm{q} = 2$. Evolution of: magnetic dipole g_1^0, inclination I, kinetic energy E_k, magnetic energy E_m, and magnetic energy of the inner core $E_{m\,\mathrm{core}}$

observable spectrum of the poloidal geomagnetic field at CMB decays as $\sim e^{-0.1n}$. Observations of the higher wave numbers n are noisy due to the mantle conductivity. Even a slow decay of the magnetic spectrum makes the geodynamo problem difficult for simulations. Estimates of the integral spectrum over the volume of the kinetic and magnetic energies reveals the existence of a maximum of the kinetic and magnetic energies at the small scales $\sim \mathrm{E}^{1/3}$ [16, 17] and the application of superdiffusion cannot be justified.

Another point is the distributions of the magnetic energy in the inner and outer parts of the core and their ratio. To the best of our knowledge, the volume of the Earth's inner core is only 4% of the volume of the entire core, while the ratio of the magnetic energies is of order $\sim 10^{-3}$, which corresponds to the ratio of energy densities of $\sim 10^{-1}$. That is why the influence of the inner core should only be a second-order effect (see, also [17]) manifesting itself only in a change of the hydrodynamics of the liquid core and in damping of the reversals and excursions with a typical time scale shorter than 10^3 years [8]. However, in many of our simulations (including those illustrated in Figure 2), the evolution of the magnetic energy of the inner core $E_{m\,core}$ correlates with the behavior of the virtual dipole of the magnetic field (VGP) presented by the first Gauss coefficient g_1^0 at CMB[5]. As a result, reversals occur when the magnetic energy of the inner core is small.

During five diffusion times (Figure 2), there were a few reversals and excursions as well as a few short events at which VGP oscillated in the equator plane. The ratio of duration of the longest and shortest intervals of the same polarity is more than one order. Between the reversals, the inclination I of VGP is about 70°, which is close to that of the Earth (I_{Earth}=76°). Recall that in geomagnetism [2] the inclination is defined by the first Gauss coefficients as $I = \dfrac{\pi}{2} - \arccos\left(\dfrac{g_1^0}{\sqrt{g_1^{0\,2} + g_1^{1\,2} + h_1^{1\,2}}}\right)$.

The Gauss spectrum of the magnetic field at ICB shows a predominance of higher harmonics. Its maximum is at $l = 4$, close to the scale of the convective roles (see Figure 3). Meanwhile, the ratio R of the dipole to quadrupole modes at the Earth's surface is ~ 10, close to geophysical observations. The magnetic field shows the dipole structure (see figure 4), but the amplitude of higher harmonics is very large.

We also present the trajectory of VGP (see Figure 5). In accordance with the paleomagnetic observations [18], the VGP path reveals chaotic precession without any certain clock- or counter-clockwise direction of precession in the vicinity of the poles. A small shift of the mean position of VGP relative to the south geographic pole is probably due to the shortness of the time interval of simulations.

3.2. The fixed temperature at ICB and the heat flux at CMB. Regime II. Another regime of the thermal conditions relevant to geophysics is a fixed temperature at ICB, $T_{\mathrm{ICB}} = 0$, with a fixed heat flux at the outer boundary, $\left.\dfrac{\partial T}{\partial r}\right|_{\mathrm{CMB}} = -1$, and the heat sources uniform over the shell volume: $G(r) = 3$. This gives $T_0(r) = 1 + r_{\mathrm{ICB}}^2/2 - r^2/2$ (Figure 1). In this regime, with $\nabla T_0(r) = -r$, convection is shifted in the

[5]Recall (see, e.g., [2]) that the solenoidal magnetic field $\mathbf{B}$ at CMB, due to the vacuum conditions, can be represented in the form $\mathbf{B} = -\nabla U$, where the scalar potential U for $r > 1$

$$U(r,\,\theta,\,\varphi) = r^{-n-2} \sum_{l=1}^{\infty} \sum_{m=0}^{l} (g_l^m \cos m\varphi + h_l^m \sin m\varphi) P_l^m(\cos(\theta))$$

is a solution to the Laplace equation $\Delta U = 0$. Here P_l^m is the associated Legendre polynomial and g_l^m, h_l^m are the Gauss coefficients.

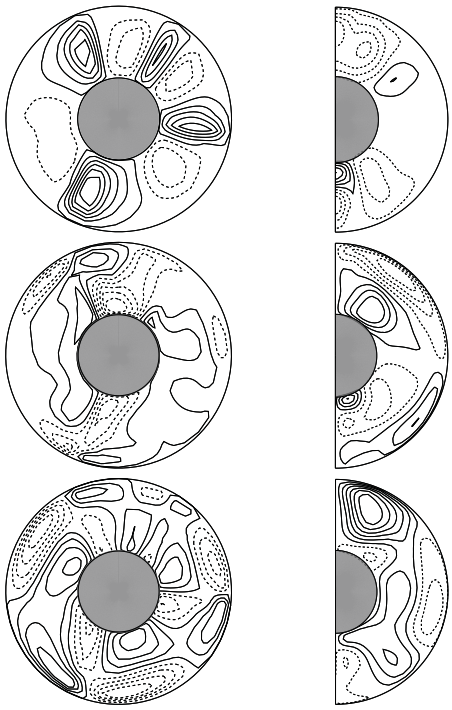

Fig. 3. For the same parameters as in Fig. 2. Equatorial section (left column) and axisymmetric part in meridional section of **V**. Minimal and maximal values for the first line $(-62.0, 128.8)$, $(-28.0, 31.9)$, for the second $(-63.2, 34.6)$, $(-22.3, 31.9)$ and for the third line $(-90.3, 72.7)$, $(-11.7, 39.9)$

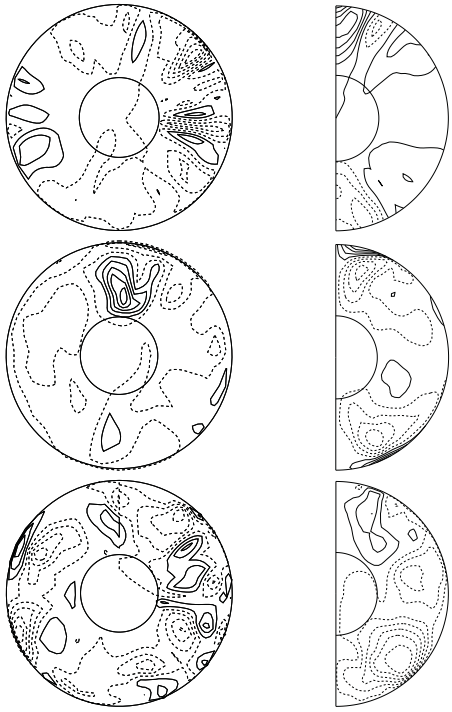

Fig. 4. For the same parameters as in Fig. 2. Equatorial section (left column) and axisymmetric part in meridional section of **B**. Minimal and maximal values for the first line $(-4.16, 2.02)$, $(-1.87, 2.52)$, for the second $(-1.16, 2.29)$, $(-1.11, 1.04)$ and for the third line $(-1.93, 1.21)$, $(-.87, 0.40)$

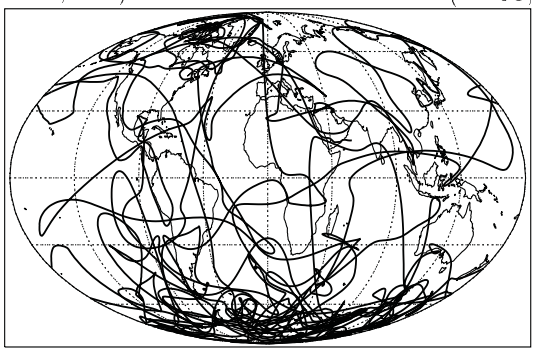

Fig. 5. Mollweide projection for VGP wander

CMB direction, which directs the system to a state where the length of the time period with small inclination I increases (Figure 6). However, there are some time periods with I comparable with the typical geophysical value, but on average the values of I are quite moderate.

As in the previous case, the evolution of the magnetic energy of the solid core follows the evolution of the magnetic dipole at CMB, so that reversals take place when the magnetic field in the solid core is weak. The value of R at CMB is close to unity. This regime resembles the magnetic field of the Giant planets (Neptune and Uranus), where I is about 50° [2]. To get closer to the geostrophical regime, one needs to decrease the Ekman number E (or to increase Pr, [17]); in this way the influence of the boundary conditions can be decreased.

3.3. Stratification. Regime III. In addition to these two unstable regimes of thermal convection, the uncertainty of geophysical parameters admits the stable regime for which the outer part of the liquid core is stratified [19]. Having in mind that the equation for the light fraction in the compositional model has the same structure as the heat-flux equation Eq. (6) [19], we can mimic this situation in the Boussinesq model as well, setting $\dfrac{\partial T_0}{\partial r} > 0$ in the outer part of the spherical shell. The same situation can also occur in an inelastic model

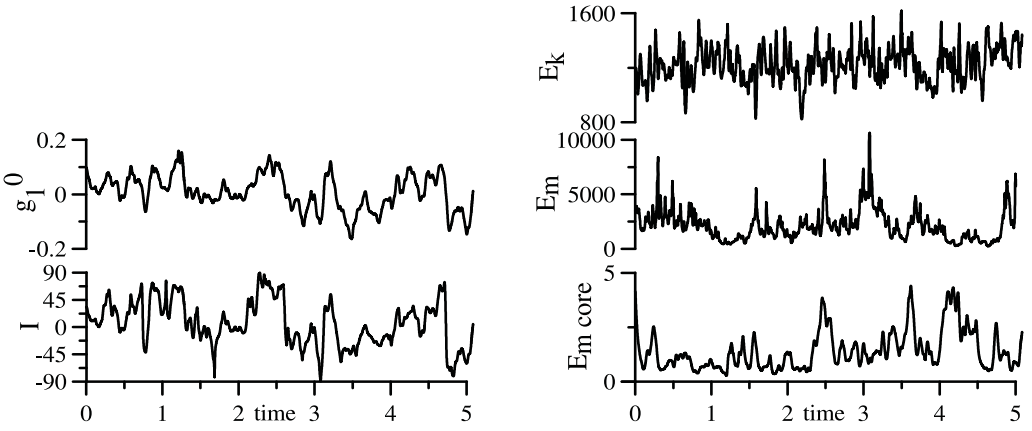

Fig. 6. Regime II, $\mathrm{E} = 3 \cdot 10^{-3}$, $\mathrm{Pr} = 1$, $\mathrm{Ra} = 10^3$, $\mathrm{q} = 4$. Evolution of: magnetic dipole g_1^0, inclination I, kinetic energy E_k, magnetic energy E_m, and magnetic energy of the inner core $E_{m\,\mathrm{core}}$

for the pure thermodynamic problem, where the adiabatic cooling is taken into account [19].

To simulate this regime, we propose $T_0(r) = \left(1 + r_{\mathrm{ICB}}^2/2 - r^2/2\right)(1-r) + \alpha r^2 (r - r_{\mathrm{ICB}})/2$ (Figure 1), where the choice of $\alpha = -2\left(-r_{\mathrm{ICB}} + r_{\mathrm{ICB}}^2 + 3\right)/(r_{\mathrm{ICB}}^2 - 4)$ provides a change of the sign of $\dfrac{\partial T_0}{\partial r}$ in the middle of the convective shell $r_m = (r_{\mathrm{ICB}} + r_{\mathrm{CMB}})/2$. This temperature profile is equivalent to

$$G(r) = \frac{9 r r_{\mathrm{ICB}}^2 - 12 r + 6 r^2 r_{\mathrm{ICB}}^2 + 60 r^2 - 2 r_{\mathrm{ICB}}^2 - 8 + r_{\mathrm{ICB}}^4 - 12 r_{\mathrm{ICB}} r^2 - 6 r r_{\mathrm{ICB}}^3 - 18 r_{\mathrm{ICB}} r}{r\left(r_{\mathrm{ICB}}^2 - 4\right)}$$

with $T_{ICB} = 1 - r_{\mathrm{ICB}}$, we get $\left.\dfrac{\partial T}{\partial r}\right|_{CMB} = -1/2 - r_{\mathrm{ICB}}^2/2 + \alpha(1 - r_{\mathrm{ICB}}) + \alpha/2$.

As in the case of Regime II, the temperature gradient shifts the convection away from the ICB. On the other hand, a positive temperature gradient near CMB suppresses convection in this region. In fact, for an observer at the planetary surface, this situation should be similar to an increase of the mantle's thickness and of its corresponding screening: the higher harmonics of the magnetic field are sufficiently damped as $\sim r^{-l-2}$. In this sense one can expect that for the dipole magnetic field generation, this regime is somewhere between the regimes I and II. Meanwhile, the numerical simulations did not reveal any significant difference to the regime II, except that $R = 2$ at CMB. This is because in all our regimes, convection concentrates near ICB (so that $\mathrm{Pr} = 1$) and stratification of the outer part of the liquid core does not change the general situation. However, for the fully turbulent regime (where vigorous convection will occupy the whole volume of the shell) as well as for the compositional convection regime (when $\mathrm{Pr} \ll 1$ and columnar convection will be exchanged by the inertial waves trapped in the equatorial region [20]), the influence of stratification can be of greater importance.

4. Convection in a thin shell. For comparison, we consider the regime with twice the radius of the inner core, r_{ICB}. This geometry corresponds to the convective zone of the Sun as well as to the cores of some Giant planets. For the Sun, however, the other parameters are also quite different from the Earth, so we consider only the relevance of this regime for Uranus and Neptune. These planets are characterized by the small inclination $I = 34°$ (Uranus) and $I = 47°$ (Neptune) as well as by the small value of $R \sim 1$ [2]. In order to understand this difference, we note that in the dynamo models the forces in rotating shells exhibit two kinds of symmetry: the axisymmetric symmetry of rotation (Coriolis force) and the spherical symmetry of gravity (Archimedean forces). The variation of the ratio of these forces may change the symmetry of the generated magnetic field. This consideration leads us to a conclusion that the influence of rotation in these two planets is not so large as in the Earth. Due to uncertainty of the parameters for these planets, this phenomenon allows slightly different explanations.

The first one was proposed in terms of the early $\alpha^2\omega$-models [21], which gives a larger value of I than the $\alpha\omega$-dynamo model used traditionally in geodynamo. Large-scale simulations based on 2.5-models, supported this proposition [22]. In both the cases, the role of the differential rotation was smaller than it appears to be in the Earth's core.

In the recent paper [23], the authors offer another explanation of this phenomenon. They introduce the idea of a stratified convection in the bottom layer of the liquid core, which in turn reduces the differential rotation. As a result, this model produces a spectrum of the magnetic field comparable with observations. Unfortunately, our present knowledge of the interior of the planets is not detailed enough for any strict conclusions on this

subject[7].

Here we present simulations according to the first scenario, with an increased Rayleigh number and with a sufficiently large Ekman number; in contrast to [22], simulations are performed in a thin shell ($r_{\mathrm{ICB}} = 0.67$) with the inner core of the same conductivity as the outer part (see geometry and typical maps of the fields in Figure 7). The choice of such a large value of the Ekman number gives the proper ratio of the Archimedean and Coriolis forces to obtain the desired magnetic spectrum. A decrease of the shell thickness causes a general decrease of scales of the fields.

We started our simulations from the typical geophysical state, with a dominating dipole field and large magnetic energy of the inner core (see Figure 8).

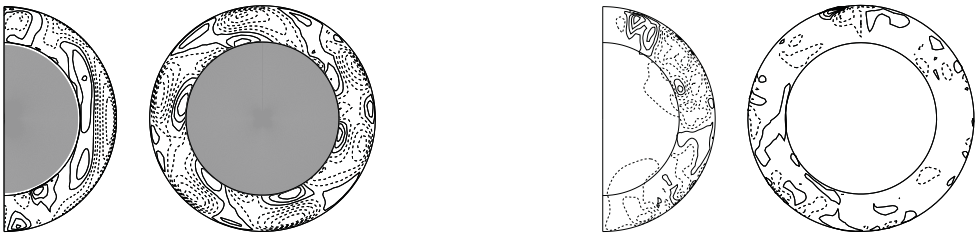

Fig. 7. Regime II, $r_{ICB} = 0.67$, $\mathrm{E} = 3 \cdot 10^{-4}$, $\mathrm{Pr} = 0.1$, $\mathrm{Ra} = 10^3$, $\mathrm{q} = 8$ on the grid $65 \times 65 \times 64$. Meridional (left column) and equatorial section (right column) of the V_φ-componet (upper line) and B_φ-componet (bottom line) of the fields. Minimal and maximal values of the velocity: $(-102, 67)$, $(-112, 62)$ and magnetic $(-0.14, 0.16)$, $(-1.0, 1.5)$ fields

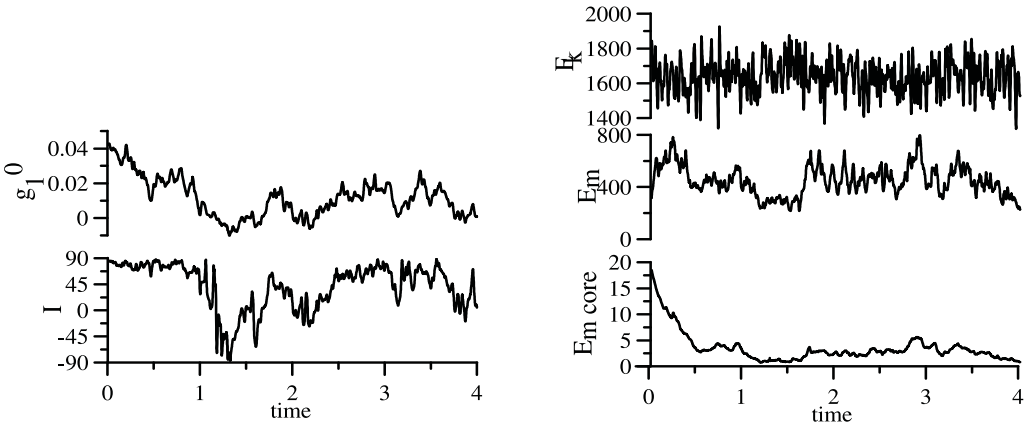

Fig. 8. Regime I, $r_{ICB} = 0.67$, $\mathrm{E} = 10^{-3}$, $\mathrm{Pr} = 1$, $\mathrm{Ra} = 3 \cdot 10^2$, $\mathrm{q} = 5$. Evolution of: magnetic dipole g_1^0, inclination I, kinetic energy E_k, magnetic energy E_m, and magnetic energy of the inner core $E_{m\,\mathrm{core}}$

After an intermediate regime without reversals, the system came to the state with a smaller value of the magnetic energy of the inner core, $E_{m\,\mathrm{core}}$, and the reversals appeared. The mean level of I decreased to $\sim 50°$, comparable with that in the Giant planets.

5. Discussion. Our analysis of the simulated magnetic spectrum at the planetary surface shows that this spectrum is not sufficient to get unambiguous information about the mean features of MHD flows in a liquid core. Although the reversals of the magnetic field are a prominent phenomenon and up to now the study of their morphology is a subject of continuous debates in the theory of paleomagnetism [18], they give little information on the magnetohydrodynamics of a liquid core.

There are many reasons for such a conclusion. One of them is that the dipole mode at CMB is only two times larger than the quadrupole mode. In this regard, one of the simple models of reversals and excursions is correlation and anticorrelation of the dipole and quadrupole oscillations. The first one gives us the full inversion. In the second case, anticorrelation prohibits the full reversal and the excursion takes place [17]. This situation is the subject of the 2.5 models of reversals [24]. Further, and more important, the invisible toroidal part of the magnetic field and the mean poloidal part in the shell volume have spectra quite different [16] from that of the surface fields. Spectra in the volume have a maximum in the higher wave numbers. Usually, during the reversals

[7] According to [17], application of the stress-free boundary conditions for the velocity field causes increase of differential rotation and also provide sufficient generation of the magnetic field.

the total magnetic energy should not decrease. This is a reason why correlation of reversals and excursions with the processes in the inner core is so difficult to reveal. Note that the axisymmetric models (like, e.g., [7]) would overestimate the role of the large-scale magnetic fields, so that the dipole mode would penetrate to the inner core and introduce additional connection of two parts of the core. On the other hand, as it follows from our analysis, this effect is present in the 3D model also: the magnetic field in the inner core and at CMB are coupled systems and reveals significant correlation. However, in the limit of the high Rayleigh numbers, when vigorous convection exists, this coupling may be sufficiently decreased.

Acknowledgements. The first author is grateful to the Central Institute for Applied Mathematics (ZAM) of Forshungszentrum in Jüulich for hospitality. This work was supported by the INTAS foundation (grant 03–51–5807) and the Russian Foundation for Basic Research (grant 03–05–64074).

References

1. *Zeldovich Ya.B., Ruzmaikin A.A., Sokoloff D.D.* Magnetic fields in astrophysics. New York: Gordon and Breach. 1983.
2. Geomagnetism. Ed. by Jacobs J.A. Vol. 2, 3. New York: Academic Press. 1988.
3. *Jones C.A.* Convection-driven geodynamo models // Phil. Trans. R. Soc. London. 2000. **A 358**. 873–897.
4. *Kono M., Roberts P.* Recent geodynamo simulations and observations of the geomagnetic field // Reviews of Geophysics. 2002. **40**, N 10. B1–B41.
5. *Hejda P., Reshetnyak M.* Control volume method for the dynamo problem in a sphere with the free rotating inner core // Studia geoph. et. geod. 2003. **47**. 147–159.
6. *Hejda P., Reshetnyak M.* Control volume method for the thermal convection problem in a rotating spherical shell: test on the benchmark solution // Studia geoph. et. geod. 2004. **48**. 741–746.
7. *Hollerbach R., Jones C.* Influence of the Earth's inner core on geomagnetic fluctuations and reversals // Nature. 1993. **365**. 541–543.
8. *Wicht J.* Inner-core conductivity in numerical dynamo simulations // Phys. Earth Planet. Inter. 2002. **132**. 281–302.
9. *Christensen U.R., Aubert J., Cardin P., Dormy E, Gibbons S., Glatzmaier G.A., Grote E., Honkura Y., Jones C., Kono M., Matsushima M., Sakuraba A., Takahashi F., Tilgner A., Wicht J., Zhang K.* A numerical dynamo benchmark // Phys. Earth Planet. Inter. 2001. **128**. 25–34.
10. *Krause F., Rädler K.-H.* Mean field magnetohydrodynamics and dynamo theory. Berlin: Akademie-Verlag, 1980.
11. *Patankar S.V.* Numerical heat transfer and fluid flow. New York: Taylor & Francis, 1980.
12. *Sarson G.R., Jones C.A., Longbottom A.W.* The influence of the boundary region on the geodynamo // Phys. Earth Planet. Inter. 1997. **101**. 13–32.
13. *Glatzmaier G.A., Coe R.S., Hongre L., Roberts P.* The role of the Earth's mantle in controlling the frequency of geomagnetic reversals // Nature. 1999. **401**. 885–890.
14. *Glatzmaier G.A., Roberts P.H.* A three-dimensional convective dynamo solution with rotating and finitely conducting inner core and mantle // Phys. Earth Planet. Inter. 1995. **91**. 63–75.
15. *Wicht J., Olson P.* A detailed study of the polarity reversal mechanism in a numerical dynamo model // Geochemistry, Geophysics, Geosystems. 2004. **5**, N 3. 1–23.
16. *Kutzner C., Cristensen U.R.* From stable dipolar towards reversing numerical dynamos // Phys. Earth Planet. Inter. 2002. **131**. 29–45.
17. *Simitev R.* Ph.D. Thesis: Convection and magnetic field generation in rotating spherical fluid shells. Bayreuth: University of Bayreuth, 2004. http://www.phy.uni-bayreuth.de/theo/tp4/members/simitev.html
18. *Jacobs J.A.* Reversals of the Earth's magnetic field. 2nd edition. Cambridge: Cambridge University Press, 2004.
19. *Braginsky S.I., Roberts P.H.* Equations governing convection in the Earth's core and the geodynamo // Geophys. Astrophys. Fluid Dynamics. 1995. **79**. 1–97.
20. *Zhang K., Busse F.H.* On the onset of convection in rotating spherical shells // Geophys. Astrophys. Fluid. Dyn. 1987. **39**. 119–147.
21. *Ruzmaikin A.A., Starchenko S.V.* On the origin of Uranus and Neptune magnetic fields // Icarus. 1991. **93**. 82–87.
22. *Cupal I., Hejda P., Reshetnyak M.* Dynamo model with thermal convection and free-rotating inner core // Planetary and Space Science. 2002. **50**. 1117–1122.
23. *Stanley S., Bloxham J.* Convective-region geometry as the cause of Uranus' and Neptune's unusual magnetic fields // Letters to Nature. 2004. **428**. 151–153.
24. *Sarson G.R., Jones C.A.* A convection driven geodynamo reversal model // Phys. Earth Planet. Inter. 1999. **111**. 3–20.

Received 19 December 2004